PHYSICAL REVIEW B **92**, 184513 (2015)

Robust determination of the superconducting gap sign structure via quasiparticle interference

P. J. Hirschfeld,[1] D. Altenfeld,[2] I. Eremin,[2,3] and I. I. Mazin[4]
[1]*Department of Physics, University of Florida, Gainesville, Florida 32611, USA*
[2]*Institut für Theoretische Physik III, Ruhr-Universität Bochum, D-44801 Bochum, Germany*
[3]*Kazan Federal University, Kazan 420008, Russian Federation*
[4]*Code 6393, Naval Research Laboratory, Washington, DC 20375, USA*

(Received 30 July 2015; revised manuscript received 28 September 2015; published 30 November 2015; corrected 4 November 2016)

Phase-sensitive measurements of the superconducting gap in Fe-based superconductors have proven more difficult than originally anticipated. While quasiparticle interference (QPI) measurements based on scanning tunneling spectroscopy are often proposed as definitive tests of gap structure, the analysis typically relies on details of the model employed. Here we point out that the temperature dependence of momentum-integrated QPI data can be used to identify gap sign changes in a qualitative way, and present an illustration for $s_{\pm}$ and s_{++} states in a system with typical Fe-pnictide Fermi surface.

DOI: 10.1103/PhysRevB.92.184513 PACS number(s): 74.20.−z, 74.70.Xa, 74.62.En

I. INTRODUCTION

There is considerable indirect evidence, but currently no "smoking gun," indicating that most, if not all, of the Fe-based superconductors condense into a superconducting state that has A_{1g} symmetry but changes sign between electron and hole pockets. This is indeed the prediction of spin fluctuation theory [1] that follows from the simple argument that the pairing interaction, proportional to the magnetic susceptibility, is repulsive and peaked at a wave vector $\mathbf{Q}$, which nearly nests these pockets. The simplest version of this state, conventionally referred to as the $s_{\pm}$ state, is isotropic on each Fermi surface pocket with opposite signs for electron and hole sheets [2]. The actual gap function realized in Fe-based superconductors (SCs) is in many cases thought to be highly anisotropic and even possess nodes, but may still be considered $s_{\pm}$ as long as the average sign on electron pockets is opposite that on hole pockets.

Arguments against the $s_{\pm}$ picture have been given as well. If orbital fluctuations dominate spin fluctuations, a state with equal sign on all pockets, denoted s_{++}, is favored [3]. In addition, when either hole or electron pockets disappear from the vicinity of the Fermi level, d-wave pairing may be enhanced [4]. Thus, as in the cuprates, the determination of the gap symmetry and structure is important as a clue to the underlying mechanism of superconductivity. As discussed in Ref. [1], this task is not as straightforward as in the cuprates due to the multiplicity of Fermi surface sheets. While many tests of $s_{\pm}$ pairing symmetry have been proposed, all seem to rely on specialized theoretical assumptions or are applicable only to certain systems. The phase-sensitive probes that proved so decisive in the identification of d-wave symmetry in the cuprates are much less useful in the Fe-based superconductors, due to the fact that both $s_{\pm}$ and s_{++}-wave symmetries belong to the same A_{1g} irreducible representation, and the difficulty of fabricating junctions with controlled properties. A general *qualitative* test of another type that could distinguish an $s_{\pm}$ pair state from others would be extremely useful.

One promising technique in this regard is quasiparticle interference, or Fourier transform scanning tunneling microscopy (FT-STM). This probe measures the wavelengths of Friedel oscillations caused by disorder present in a metallic or superconducting system, which in principle contain information on the electronic structure of the pure system. These wavelengths appear in the form of peaks at particular wave vectors $\mathbf{q}(\omega)$, which disperse with STM bias $V = \omega/e$. There is no reliable quantitative theory of quasiparticle interference, in general because the sources of disorder, exact impurity potentials, and $\mathbf{k}$ dependence of the tunneling matrix elements are unknown. However, the positions of the $\mathbf{q}$ do not depend on these effects and are related only to the electronic structure, including the superconducting gap function.

The notion that subsets of these $\mathbf{q}$ that connect gaps of equal or opposite sign on the Fermi surface can be enhanced or not according to the type of disorder was introduced by Nunner *et al.* [5]. Pereg-Barnea and Franz [6] then proposed that a disordered vortex lattice should behave like a set of localized order parameter suppression scattering centers, and could be used to introduce disorder in a controlled fashion with an external field. This experiment was performed on the cuprate superconducting compound, $Ca_{2-x}Na_xCuO_2Cl_2$, by Hanaguri *et al.* [7], who showed that certain quasiparticle interference (QPI) $\mathbf{q}$ were indeed enhanced or suppressed by the field, in a manner apparently consistent with d-wave pairing.

This experiment was attempted in the Fe-based superconductors on a a Fe(Se,Te) superconducting sample near optimal doping by Hanaguri *et al.* [8], who identified three interband scattering wave vectors $\mathbf{q}$: one associated with hole-electron scattering (the smallest momentum), and two associated with two different electron-electron scatterings. The last two features were enhanced in the presence of magnetic field with respect to the first one, which led the authors to conclude that the hole and the electron pockets have opposite signs of the order parameter, as expected in the $s_{\pm}$ model [9,10]. Some caveats regarding the interpretation, associated with the fact that two of the wave vectors coincide with Bragg peaks, were discussed in Ref. [1], and there are other issues that we consider below. More recently, Chi *et al.* [11] measured QPI on LiFeAs in zero external field, studying the bias dependence of a large $\mathbf{q}$ peak corresponding to interband and a small $\mathbf{q}$ peak corresponding to intraband scattering, arguing that upon moving from large to small bias, the fact that one was suppressed while the other enhanced could be consistent only with $s_{\pm}$ pairing. This is also an argument of the qualitative type,

but because the actual intensity dependence of the peaks as a function of bias was in fact nonmonotonic, and because there is currently no well-founded theory to support this conclusion, the interpretation is uncertain.

In fact, while QPI measured by FT-STM is, in principle, a very powerful qualitative tool, it is nearly useless as a quantitative one. This is because, while the poles of the response function (**q**-spot positions) are universal, the weights are not, but depend on the type, strength, and range of the scatterers (not generally known), as well as the details of the electronic structure (including the gap), and the z position at which the local density of states (LDOS) is calculated. The actual pattern calculated in even the most sophisticated theories then generally bears little detailed resemblance to the measured STM Fourier intensities (for a discussion of some of the causes see Ref. [12]), and identifying the symmetry or structure of the gap function by a comparison of the intensity patterns is similar to determining the age of a model from a Picasso cubist painting.

The situation is further exacerbated by advanced mythology that has formed over years about QPI. A part of this mythology involves belief that the QPI spectra are defined by the geometry of the Fermi surface in a nesting-like way, another part that in the superconducting state these spectra are proportional to coherence factors, and that magnetic and nonmagnetic impurities have opposite effect on QPI. While this mythology has been partially rectified in some papers, it has not become generally appreciated, and some myths still persist.

A systematic summary of the established facts is badly needed, and we shall provide it later in the paper. But, the main purpose of this paper is to find a clean qualitative way to design a QPI experiment capable of distinguishing $s_{\pm}$ from other pairings, and in general to identify sign-changing gaps in an unconventional superconducting system. We argue that the best way is to measure the intensity of integrated interband scattering peaks in the Fourier transformed density of states, antisymmetrized with respect to STM bias, as a function of temperature. Then the integrated weights of the set of **q** corresponding to sign-changing scatterings display a strong enhancements only for this channel; furthermore these qualitative distinctions are robust against the strength of the scattering. We conclude that while the general theory of QPI in unconventional superconductors has many pitfalls, this particular consequence of pairing sign change is robust and can be used to unambiguously identify $s_{\pm}$ pairing if this type of distinction between intra- and interband pairing **q** peaks is observed.

II. FORMALISM

Here we present a model that captures all the qualitative features of the general two-band case, but allows analytical evaluation of the density of states. We are interested in the density of states in a two-band superconductor of isotropic s_{++} or $s_{\pm}$ type in the presence of disorder of various kinds. Here, following the tradition, we use the words "one-band" and "two-band" for materials with arbitrary complex normal electronic structure, but with the superconducting order parameter Δ that can be approximated by a single value for all states on the Fermi level, or by two different values, depending on the location in the Brillouin zone.

A. One-band problem

We first remind the reader of the one-band problem. We assume a random distribution of N_I pointlike impurities at sites $\mathbf{R}_i$ with $i = 1,\ldots,N_I$. The LDOS can be formally decomposed $\rho(\mathbf{r},\omega) = \rho_0(\omega) + \delta\rho(\mathbf{r},\omega)$, where ρ_0 is the DOS of the homogeneous superconductor, and $\delta\rho$ is the local change in the DOS due to disorder given exactly by

$$\delta\rho(\mathbf{r},\omega) = -\frac{1}{\pi}\,\mathrm{Im}\sum_{i,j=1}^{N_I}[\hat{G}^0(\mathbf{r}-\mathbf{R}_i)\hat{T}_{ij}\hat{G}^0(\mathbf{R}_j-\mathbf{r})]_{11},$$

where the ω dependence is suppressed for simplicity, $\hat{T}(\omega)$ is the $2N_I \times 2N_I$ many-impurity T matrix (the factor of two is due to spin), $\hat{G}^0(\mathbf{r},\omega)$ is the bare advanced electron Green's function $\hat{G}^0(\mathbf{r},\omega) = \sum_{\mathbf{k}} \hat{G}^0(\mathbf{k},\omega)\exp(i\mathbf{k}\cdot\mathbf{r})$, $\hat{}$ refers to Nambu space, and $[\ldots]_{\alpha\beta}$ are Nambu spinor indices. The T matrix represents the solution to the scattering problem $\hat{T} = \hat{V} + \hat{V}\hat{G}^0\hat{T}$ for N impurities of identical potential $\hat{V}_i$ at $\mathbf{R}_i$. Note that here we have already made an important approximation, neglecting Umklapp processes (that is, using one argument in the bare Green's functions instead of two). We will discuss this approximation in Appendix A1.

It was shown in Refs. [13] and [14] that the poles of the many-impurity response (change in LDOS) are identical to the single-impurity problem, although the weights may differ substantially. In addition, in the limit of weak impurity potentials, the response for the two problems are identical modulo a disorder-dependent factor [13]. For clarity, we therefore consider the simpler problem and present results for a single impurity, and replace the full T matrix by $\hat{T}_{ij} \to \hat{t}_i\delta_{ij}$, with $\hat{t}_i = [1 - \hat{V}_i\hat{G}^0(\mathbf{r}=0)]^{-1}\hat{V}_i$.

It was shown in Ref. [15] for simple metals, and generalized to unconventional superconductors by Ref. [16], that information about the pure electronic system could be extracted from STS measurements by examining the Fourier transform of dI/dV maps. The Fourier transform of the LDOS is $\rho(\mathbf{q},\omega) = \sum_{\mathbf{r}\in L\times L} e^{-i\mathbf{q}\cdot\mathbf{r}}\rho(\mathbf{r},\omega)$, where $L \times L$ is a square set of L^2 positions at which measurements are made, and $\mathbf{q} = 2\pi(m,n)/L$ are vectors in the associated reciprocal lattice. The result for a single band is then

$$\begin{aligned}\delta\rho(\mathbf{q},\omega) &= \frac{1}{\pi}\,\mathrm{Im}\sum_{\mathbf{k}}[\hat{G}^0(\mathbf{k},\omega)\hat{t}(\omega)\hat{G}^0(\mathbf{k}+\mathbf{q},\omega)]_{11}\\ &= \frac{1}{2}\mathrm{Tr}\,\mathrm{Im}\sum_{\mathbf{k}}(\tau_0+\tau_3)\hat{G}^0(\mathbf{k},\omega)\hat{t}(\omega)\hat{G}^0(\mathbf{k}+\mathbf{q},\omega).\end{aligned} \tag{1}$$

Here, $\hat{\tau}_i, i = 0,3$ are the Pauli matrices spanning Nambu space.

B. Two-band model: q-integrated LDOS peaks

Several works have already established the basic generalization of (1) to multiband models [10,17–21]. The qualitatively new aspect is that impurities can scatter quasiparticles between bands, and if the state is of $s_{\pm}$ type, between bands where the superconducting order parameter $\Delta_{\mathbf{k}}$ has opposite

sign. The various types of scattering processes can then be classified according to whether they connect portions of the Fermi surface with different gap sign or not, as was done previously in the cuprates [5,7,22]. Without loss of generality for our qualitative purposes, we consider a pointlike scatterer with Nambu and band space potential $\hat{V}_{\mu\nu}(\mathbf{k},\mathbf{k}') \simeq \sum_\alpha V^\alpha_{\mu\nu}\tau_\alpha$, with band indices $\mu,\nu = h,e$, where h and e are just band indices, although for typical Fe pnictides they correspond to hole and electron pockets, and τ_3 and τ_1 correspond, respectively, to nonmagnetic and Andreev scattering, which we discuss separately. Weak, purely magnetic scatterers do not couple to the spin-averaged local density of states measured by a typical STM experiment, so we ignore this possibility for the moment (while in Ref. [7] it was incorrectly suggested that magnetic scattering contributes to QPI with a different coherence factor, this mistake was corrected in a later paper by the same authors [23]). Note that the generalization to 3 or more bands in the Fe-based systems is straightforward and should not change our basic conclusions.

In the Fe-based systems, the Fermi pockets corresponding to bands 1 and 2 are well-separated in momentum space and generally have small radius. It is therefore reasonable to expect that isolated spots of scattering intensity will be observed generically at small $\mathbf{q}$, corresponding to intraband scattering processes, and at large q, corresponding to interband [11]. The intraband term is a simple sum of the one-band expression applied to each band separately,

$$\delta\rho(\mathbf{q}\sim 0,\omega) = \frac{1}{2}\mathrm{Tr}\,\mathrm{Im}\sum_{\mathbf{k}\nu}(\tau_0+\tau_3)\hat{G}^0_\nu(\mathbf{k},\omega)\hat{t}_{\nu\nu}(\omega)\hat{G}^0_\nu(\mathbf{k}+\mathbf{q},\omega). \tag{2}$$

The form of $\hat{t}_{\mu\nu}(\omega)$ is known for simple cases [24] but can be a complicated function of the various integrated Green's function components, so we do not specify it here. Full expressions are given in Appendix A3.

Suppose now that we wish to calculate the total weight in the small $\mathbf{q}$ QPI spot as a function of frequency, defined to be

$$\begin{aligned}\delta\rho_{\mathrm{intra}}(\omega) &= \frac{1}{2}\mathrm{Tr}\ \mathrm{Im}\sum_{\mathbf{k},\mathbf{q}\sim 0,\nu}(\tau_0+\tau_3)\hat{G}^0_\nu(\mathbf{k},\omega)\hat{t}_{\nu\nu}(\omega)\hat{G}^0_\nu(\mathbf{k}+\mathbf{q},\omega)\\ &\approx \frac{1}{2}\mathrm{Tr}\ \mathrm{Im}\sum_{\mathbf{k},\mathbf{q},\nu}(\tau_0+\tau_3)\hat{G}^0_\nu(\mathbf{k},\omega)\hat{t}_{\nu\nu}(\omega)\hat{G}^0_\nu(\mathbf{k}+\mathbf{q},\omega)\\ &= \frac{1}{2}\mathrm{Tr}\ \mathrm{Im}\sum_{\mathbf{k},\mathbf{k}',\nu}(\tau_0+\tau_3)\hat{G}^0_\nu(\mathbf{k},\omega)\hat{t}_{\nu\nu}(\omega)\hat{G}^0_\nu(\mathbf{k}',\omega),\end{aligned} \tag{3}$$

where in the second step we extended the sum over the small range of $\mathbf{q}$ around $\mathbf{q}=0$ to the full Brillouin zone, since the product of two Green's functions from the same band is sharply peaked at small $\mathbf{q}$ for small ω. In the last step, we expressed the double $\mathbf{k}$ sum as independent sums over the Nambu Green's functions, which then decouple provided that t is momentum independent, as we have assumed for the moment. In the simplest approximation with a flat DOS near the Fermi level, the integrated matrix Green's function is

$$\sum_{\mathbf{k}}\hat{G}^0_\nu(\mathbf{k},\omega) \simeq i\pi\rho_\nu\frac{\omega\tau_0+\Delta_\nu\tau_1}{\sqrt{\omega^2-\Delta^2_\nu}}. \tag{4}$$

Thus one can use Eq. (4) to perform all momentum integrations in Eq. (3) and obtain closed form expressions for the intraband $\mathbf{q}$-integrated LDOS weight $\delta\rho_{\mathrm{intra}}(\omega)$ or the corresponding interband quantity describing scattering between two pockets separated by $\mathbf{q}_0$,

$$\begin{aligned}\delta\rho_{\mathrm{inter}}(\omega) &\equiv \frac{1}{2}\mathrm{Tr}\,\mathrm{Im}\sum_{\mathbf{q}\sim\mathbf{q}_0}\delta\rho(\mathbf{q},\omega)\\ &= \frac{1}{2}\mathrm{Tr}\ \mathrm{Im}\sum_{\mathbf{k},\mathbf{k}',\mu\neq\nu}(\tau_0+\tau_3)\,\hat{G}^0_\mu(\mathbf{k},\omega)\hat{t}_{\mu\nu}(\omega)\hat{G}^0_\nu(\mathbf{k}',\omega).\end{aligned} \tag{5}$$

Note that we also performed a calculation for the lattice (momentum-resolved) model with two bands, giving parabolic like electron and hole band dispersions near the Γ and the M points of the Brillouin zone. The results are shown in Sec. III. Most importantly, the main features, especially the T dependence of the antisymmetric correction to the LDOS and its frequency dependence, allowing one to distinguish s_{++} and $s_\pm$ superconducting gaps, continue to hold.

III. RESULTS: WEAK POTENTIAL SCATTERERS

A. $T = 0$ frequency dependence

To complete the solution, the t matrix for a given impurity type must be specified. Here we argue that the basic qualitative features of the QPI patterns that are sensitive to the sign change of the order parameter (or lack thereof) depend only on the Nambu space structure of the t matrix, which can be extracted by constructing the components of the conductance properly symmetrized and antisymmetrized with respect to bias. They do *not* depend on the detailed energy dependence of the complex t matrix, except insofar as impurity bound states are created within the gap. Even in this case, the question of $s_\pm$ or s_{++} can be decided by means described below.

We show this by first considering the case of constant t matrix, valid for weak (Born) impurity scattering. While in general $\hat{t}$ has several Nambu components depending on the type of scattering, superconducting state and impurity phase shift, it is instructive to focus on one Nambu component at a time. For example, if $\hat{t} = t_3\tau_3$, as, e.g., for a weak nonmagnetic scatterer, then

$$\begin{aligned}\delta\rho_{\mathrm{intra}}(\omega) &\approx -\frac{\pi^2}{2}t_3\sum_\nu\rho^2_\nu\mathrm{Im}\\ &\quad\times\frac{\mathrm{Tr}(\tau_0+\tau_3)(\omega\tau_0+\Delta_\nu\tau_1)\tau_3(\omega\tau_0+\Delta_\nu\tau_1)}{\omega^2-\Delta^2_\nu}\\ &= 0,\end{aligned} \tag{6}$$

in other words, within this approximation, there is *no change* in the small-$\mathbf{q}$ integrated Fourier transform density of states due to a nonmagnetic intraband scatterer, regardless of the relative sign of the two gaps $\Delta_{h,e}$. The same is not true in general of the interband contribution $\delta\rho_{\mathrm{inter}}(\omega) \equiv \frac{1}{2}\mathrm{Tr}\mathrm{Im}\sum_{\mathbf{q}\sim\mathbf{q}_0}\delta\rho(\mathbf{q},\omega)$,

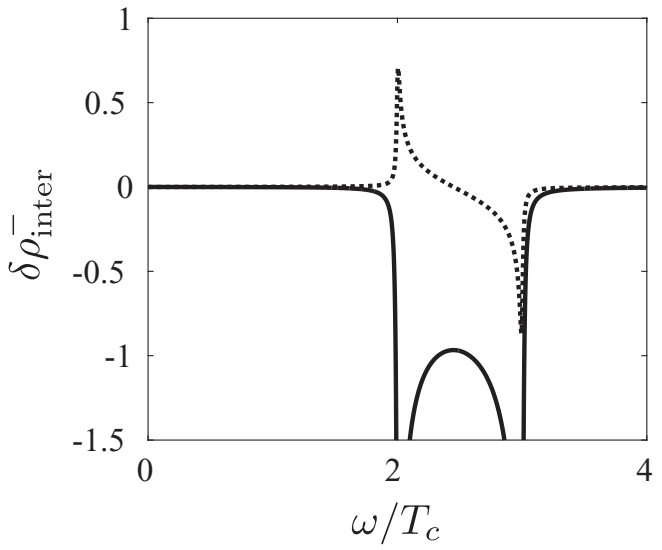

FIG. 1. Integrated interband density of states $\delta\rho_{\rm inter}/(t_3\rho_1\rho_2)$ for constant (weak) τ_3 t matrix. Gap magnitudes are $|\Delta_1|/T_c = 3$, $|\Delta_2|/T_c = 2$, and artificial broadening $\eta = 10^{-3}$. Solid line: $s_\pm$ state. Dashed: s_{++}. All other components of $\delta\rho$ are zero for this case.

where $\mathbf{q}_0$ is the wave vector connecting the two Fermi surface pockets. In this case we have, again for the τ_3 component of the t matrix,

$$\delta\rho_{\rm inter}(\omega) \approx -2\pi^2 t_3\rho_h\rho_e {\rm Im} \times \frac{{\rm Tr}(\tau_0+\tau_3)(\omega\tau_0+\Delta_h\tau_1)\tau_3(\omega\tau_0+\Delta_e\tau_1)}{\sqrt{\omega^2-\Delta_h^2}\sqrt{\omega^2-\Delta_e^2}} = -2\pi^2 t_3\rho_h\rho_e {\rm Im}\frac{\omega^2-\Delta_h\Delta_e}{\sqrt{\omega^2-\Delta_h^2}\sqrt{\omega^2-\Delta_e^2}}, \quad (7)$$

which is manifestly nonzero for $|\Delta_e| < \omega < |\Delta_h|$. Furthermore it is easy to show that in the limit when the two gap magnitudes become equal, $|\Delta_e| \to |\Delta_h|$, there are two distinct cases. For an $s_\pm$ state, ${\rm sgn}\,\Delta_h\Delta_e < 0$, $\delta\rho_{\rm inter}(\omega) = -2\pi^2\rho_1\rho_2\Delta_h\delta(\omega - |\Delta_h|)$, while for an s_{++} state, $\delta\rho_{\rm inter} \to 0$. In the more general case with $\Delta_h \neq \Delta_e$, the interband response in the $s_\pm$ case remains generically much larger than that in the s_{++} case, with weight concentrated between the two energies $\omega = |\Delta_h|, |\Delta_e|$. In Fig. 1, we plot the interband frequency-dependent $\mathbf{q}$-integrated LDOS change for a model constant τ_3 t matrix to illustrate this difference. Note not only the change in sign of the s_{++} response due to the numerator of (7), which vanishes at an energy corresponding to the the geometric mean of the two gaps in this case, but also the overall small scale.

For a realistic scatterer, the Born limit results given above are no longer adequate, and the t matrix acquires components in all Nambu channels. It is instructive to consider the response of the system to a scatterer with constant t matrix in each of these channels, even if none of these cases corresponds to a physical situation with the exception of the τ_3 (weak potential) scatterer.[1] One can define the experimentally accessible quantities

$$\rho^{(\pm)}_{\substack{\rm intra\\ \rm inter}}(\omega) = \rho_{\substack{\rm intra\\ \rm inter}}(\omega) \pm \rho_{\substack{\rm intra\\ \rm inter}}(-\omega),$$

and use them to make clear qualitative predictions for the existence or nonexistence of a strong QPI response in the various channels that are independent of the type of scatterer, as summarized in Table I. These features will also correspond to peaklike features in the T dependence of the integrated QPI intensity, as we discuss below. In particular, it is easy to see that the τ_0 component of the t matrix reverses the responses of s_{++} and $s_\pm$ compared to the τ_3 scatterer. For the intraband part, we get immediately $\delta\rho_{\rm intra}(\omega) = -\pi^2 t_0 \sum_\nu \rho_\nu^2\Delta_\nu\delta(\omega - |\Delta_\nu|)$ for both $s_\pm$ or s_{++}. The interband processes contribute 0 for an $s_\pm$ state and $-2\pi^2\rho_h\rho_e\Delta_h\delta(\omega - \Delta_h)$ for an s_{++} state. Finally, for a single impurity with constant t matrix in the τ_1 channel, one easily finds that the intraband symmetric densities of states $\delta\rho^+_{\rm intra}$ are singular. The antisymmetric interband density of states $\delta\rho^-_{\rm inter}$ vanishes identically, but the symmetric part $\delta\rho^+_{\rm inter}$ can be large. The weight is proportional to $\omega(\Delta_h + \Delta_e)$, so taking our limit $|\Delta_h| \to |\Delta_e|$ for qualitative comparison as above, we see that the s_{++} case is singular while the $s_\pm$ case vanishes.

TABLE I. Possibility of singular integrated QPI intensity (Fourier transformed density of states) in the symmetric (+) and antisymmetric (−) channels for s_{++} and $s_\pm$ superconductors. Here, τ_α indicates the presence of a strongly enhanced response for an assumed constant t matrix in the α Nambu channel, and the $\times$ indicates the absence of one. Magnetic impurities have Nambu symmetry $\tau_0\sigma_z$ and do not modulate the total LDOS within the Born approximation (see text).

		intra	inter
s_{++}	$\delta\rho^{(+)}$	τ_0,τ_1	τ_0,τ_1
	$\delta\rho^{(-)}$	$\times$	$\times$
$s_\pm$	$\delta\rho^{(+)}$	τ_0,τ_1	$\times$
	$\delta\rho^{(-)}$	$\times$	τ_3

Although a generic nonmagnetic impurity has all Nambu components of the t-matrix, which will mix these behaviors, they can be isolated to some extent by constructing the symmetrized and antisymmetrized densities of states, respectively, as suggested by Maltseva and Coleman [7,23]. This is because the τ_3 component of the t matrix generates only odd frequency changes to the density of states to all orders in perturbation theory, and the τ_0 and τ_1 component only even ones. The τ_2 component does not contribute to the change in the Fourier transformed LDOS to all orders in perturbation theory simply because of the Trace over Nambu matrices, together with the assumption that the gaps are real (i.e., appear with τ_1). Furthermore, this statement is correct even if the particle-hole symmetry is broken (i.e., the normal part of the Nambu Green's functions has an additional τ_3 component).

[1] In a d-wave superconductor, the large impurity potential limit yields $\hat{t} \propto \tau_0$, but in an s-wave system the nonvanishing integrated anomalous Green's functions generate τ_1 and τ_2 terms as well.

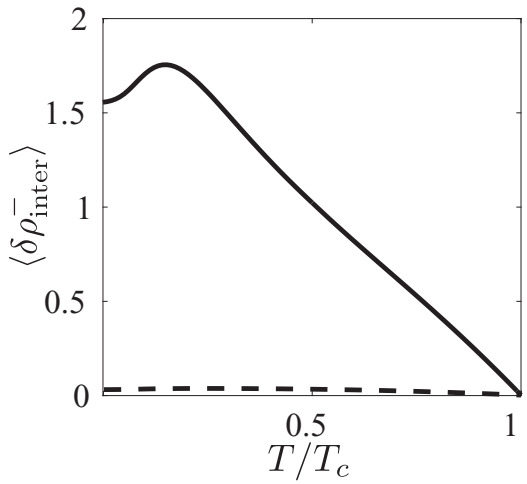

FIG. 2. Thermally averaged interband **q**-integrated LDOS change within constant density of states and constant t-matrix approximation for weak nonmagnetic scatterer with τ_3 (Born limit) potential. The external frequency Ω was taken to be 2.5 in units where $|\Delta_1|$ and $|\Delta_2|$ were 3.0 and 2.0, as in Fig. 1. Shown is antisymmetrized LDOS $\langle \delta\rho^-(\Omega)\rangle$ for s_{++} (dashed) and for $s_\pm$ state (solid). Symmetrized components are zero for both states.

B. Thermal average: STM observable

Our intention is to make clear qualitative predictions for observable quantities in STM experiments. Thus far, we have shown only the $T = 0$ results for the artificial case of a constant real t matrix. In any measurement at finite temperature, the conductance will be related to the change in LDOS $\delta\rho$ convolved with a thermal factor weighting the contribution of different electronic states to the current. The conventional result [25], translated into our notation, is

$$\langle \delta\rho^{\pm}(\Omega)\rangle \equiv \int_{-\infty}^{\infty} d\omega \delta\rho^{\pm}(\omega)\left[\frac{-\partial f}{\partial\omega}(\omega+\Omega) \pm \frac{-\partial f}{\partial\omega}(\omega-\Omega)\right]. \tag{8}$$

In Fig. 2, we plot the nonzero antisymmetrized **q**-integrated density of states for the interband QPI peak in both s_{++} and $s_\pm$ states in this simple approximation. Measurement of the antisymmetric components of the interband density of states alone should suffice to qualitatively distinguish the two states. Note that the clearest results are obtained when the STM bias corresponds to an energy between the two gap energies, which can be identified from local tunneling spectra.

It appears at first glance from Table I that measurement of the symmetrized interband **q**-integrated LDOS might also distinguish the two states. However, it is important to stress here that there is no physical impurity in the case of an s-wave superconductor corresponding to a situation where the t matrix is entirely of τ_0 type; other components of the t-matrix are mixed at strong impurity potentials. This we show below for the realistic Coulomb screened impurity potential. In particular, we will show that very little difference between s_{++} and $s_\pm$ will be observed in the symmetrized channel for realistic situations. We therefore believe that the symmetrized channel should be ignored in the analysis of STM data.

It is useful to observe that the temperature dependent average conductances predicted here bear no relation to the standard forms one might expect were quasiparticle interference really described by conventional coherence factors, as anticipated in Refs. [7] and [23]. This issue is discussed in some length in Appendix A2.

IV. GENERAL SCATTERING POTENTIALS

A. Realistic screened Coulomb potentials

The t matrix for a single impurity is given by

$$\underline{t} = \left[1 - \underline{U}\tau_3 \sum_{\mathbf{k}} \underline{G}(\mathbf{k},\omega)\right]^{-1} \tau_3 \underline{U}, \tag{9}$$

where the integrated matrix Green's function given in Eq. (4) can be further rewritten as $(\sum_{\mathbf{k}} \hat{G}(\mathbf{k},\omega))_{\nu\nu} = g_{\omega,\nu}\tau_0 + g_{\Delta,\nu}\tau_1$ for each of the bands. The scattering potential matrix $\underline{U}$ can be then separated into intraband $\hat{U}_{aa} = \hat{U}_{bb} = U_{\rm intra}\tau_0$ and the interband $\hat{U}_{ab} = U_{\rm inter}\tau_0$ term.

We have shown that a constant t matrix in the Born limit leads to a clear prediction of QPI intensities enabling one to distinguish s_{++} from $s_\pm$ states. For intermediate to strong scatterers, however, the t matrix is complex and frequency dependent, and includes τ_1 and τ_2 components in addition to τ_0 and τ_3. One may thus be concerned that our conclusions may not be general, given that one does not know *a priori* the strength of impurities giving rise to the QPI signal. We therefore present results for the full t matrix of a single impurity of arbitrary strength and intra- versus interband scattering potential, within the flat normal state DOS approximation [Eq. (4)]. Since for large q a screened Coulomb potential falls off like $1/(q_{TF}^2 + q^2)$, and screening lengths $2\pi/q_{TF}$ are of order the unit cell size, realistic interband scattering potentials are smaller than intraband potentials. We therefore begin in Fig. 3 by fixing $U_{\rm inter} = 0.2\,U_{\rm intra}$ for various strengths of $U_{\rm intra}$. To analyze these results, it is useful to identify exactly what terms distinguish s_{++} and $s_\pm$ states. In the simple pedagogical example with which we began, there were no such terms in the intraband scattering channel, Eq. (6), and one term in the antisymmetrized interband channel expression for $\delta\rho^-_{\rm inter}$ Eq. (7) proportional to $\Delta_h\Delta_e$. The full result in the general scattering potential case is given in the Appendix A3, but we find analogously that the intraband LDOS has no proportionality to terms sensitive to sign changes. In the interband channel, there are no $\Delta_h\Delta_e$ terms in the symmetrized LDOS, whereas the antisymmetrized LDOS $\delta\rho^-_{\rm inter}$ still contains only a single term proportional to

$$U_1 {\rm Im} \frac{\Delta_h\Delta_e}{\sqrt{\omega^2-\Delta_h^2}\sqrt{\omega^2-\Delta_e^2}}, \tag{10}$$

i.e., precisely the same expression as in the simpler example of the Born limit. All terms will be multiplied by the denominator of the full t matrix, of course, which also contains terms that weakly distinguish s_{++} and $s_\pm$ states, but this does not alter our qualitative conclusions.

In consequence, we find that the singular behavior of $\delta\rho^-_{\rm inter}$ in the $s_\pm$ case is preserved until the unitary limit is reached. In Sec. IV C below, we exhibit the experimentally observable consequences of this effect.

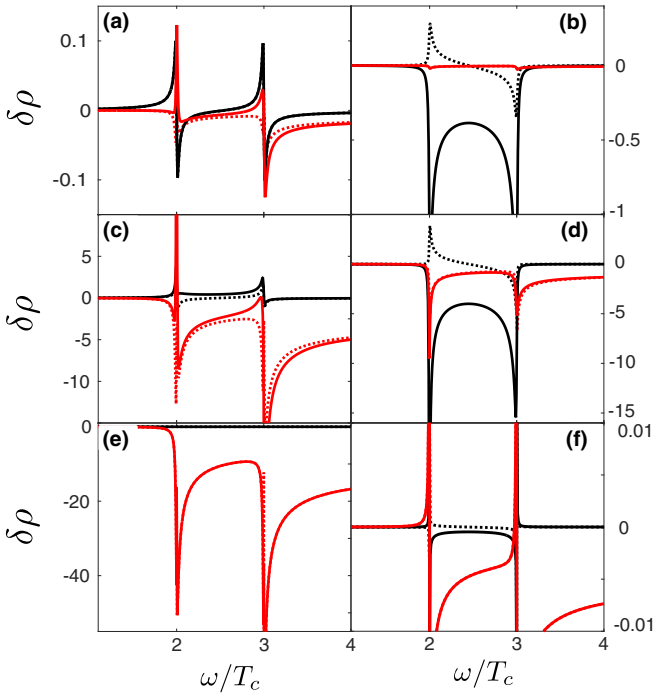

FIG. 3. (Color online) Integrated density of states components $\delta\rho^{\pm}_{\text{intra,inter}}$ for "realistic" screened Coulomb scatterers $U_{\text{inter}} = 0.2U_{\text{intra}}$, for $U_{\text{intra}} = 0.01$ [(a) and (b)], 0.2 [(c) and (d)], and 10 [(e) and (f)]. Dashed curves correspond to s_{++} state, solid curves to $s_{\pm}$. Red and black are even and odd components of the LDOS, $\delta\rho^{+}$ and $\delta\rho^{-}$, respectively. Left panels represent intraband, right panels interband scattering channels, respectively.

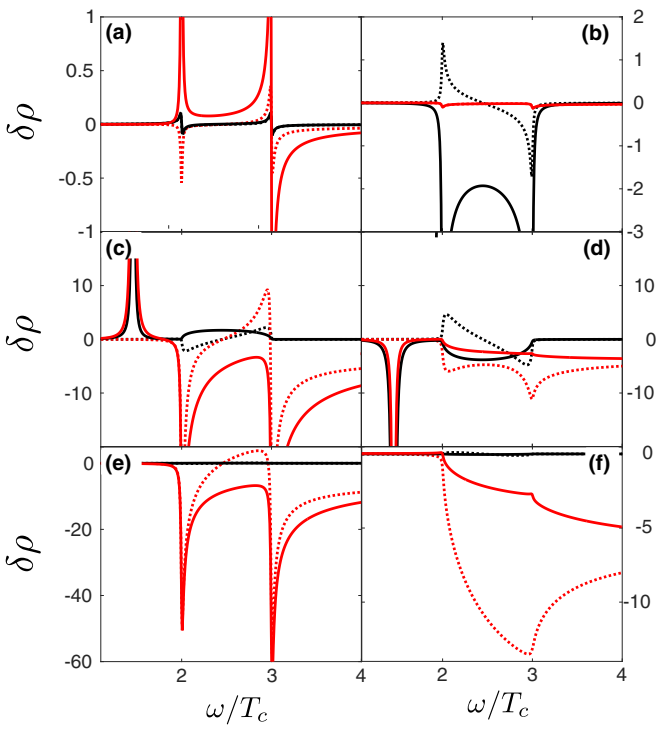

FIG. 4. (Color online) Integrated density of states components $\delta\rho^{\pm}_{\text{intra,inter}}$ for isotropic scatterers $U_{\text{intra}} = U_{\text{inter}}$ for $U_{\text{intra}} = 0.01$ [(a) and (b)], 0.2 [(c) and (d)], and 10 [(e) and (f)]. Dashed curves correspond to s_{++} state, solid curves to $s_{\pm}$. Red and black are even and odd components of the LDOS, $\delta\rho^{+}$ and $\delta\rho^{-}$, respectively. Left panels represent intraband, right panels interband scattering channels, respectively.

B. Role of bound states

In the cases discussed in Fig. 1, no impurity bound states are visible in the subgap region below $|\Delta_e| = 2$. In general, the formation of impurity bound states in a multiband system is more complicated than in a one-band superconductor, and it has been argued that such states are indeed nongeneric, requiring fine-tuning of the potential to produce a bound state below the lower gap edge [1,26]. In the two-band model, subgap bound states are found only in a very narrow interval around a line $U_{\text{inter}}(U_{\text{intra}})$ in impurity potential space which approaches $U_{\text{inter}} = U_{\text{intra}}$ for strong impurities [1]. We therefore discuss the case $U_{\text{inter}} = U_{\text{intra}}$ separately here.

Figures 4(a) and 4(b) essentially reproduce the results of Fig. 3 for a weak scatterer. With increased scattering strength, however, bound states are formed in the $s_{\pm}$ case, as seen in Fig. 4(d). If the bound state is at low energy, it steals so much weight from the coherence peak LDOS that the hierarchy of intensities represented in Table I becomes a bit difficult to distinguish. To use QPI as a definitive qualitative tool, it may therefore be necessary to consider only systems without impurity bound states in the gap, which occurs sometimes, or to mask the impurities that give rise to bound states in the spatial window used for the Fourier transform. Of course, the observation of bound states in and of itself is strong evidence for $s_{\pm}$ pairing, provided the nonmagnetic character of the impurities can be reliably assumed. If no bound states occur, the hierarchy of LDOS moments of Table I is clear [compare Figs. 3(c) and 3(d)].

In the unitary limit, Figs. 4(e) and 4(f) the bound state has already moved through the gap and the basic hierarchy is again preserved. Note that for this simple band, this limit is essentially achieved already for potentials of order T_c.

C. Finite temperatures

For transparency, we now remove from consideration those components of the **q**-integrated LDOS which are not qualitatively affected by a gap sign change, and plot in Fig. 5 the thermally averaged, antisymmetrized, interband integrated LDOS for the two states s_{++} and $s_{\pm}$, Eq. (8). Here we have used the standard BCS type T dependence for both superconducting gaps. Thermal averaging has the effect of removing many of the sharp spectral features at the gap edge, as discussed pedagogically for the case of a constant t matrix in Fig. 2 above. It is clear that the temperature dependent signal in the $s_{\pm}$ case is huge and characteristic, whereas in the s_{++} it is small and featureless. Note that the slight decrease of $\langle\delta\rho^{-}_{\text{inter}}\rangle$ occurs when the width of the peaks in the $\delta\rho^{-}_{\text{inter}}$ becomes comparable to the thermal broadening of the derivative of the Fermi function. It is also clear that the T dependencies do *not* resemble the classic BCS T dependencies arising from coherence factors in, e.g., NMR relaxation and acoustic attenuation cases (see Appendix A2). We propose that the measurement of $\langle\delta\rho^{-}_{\text{inter}}\rangle$ versus temperature is therefore the clearest way of identifying a gap sign change using QPI.

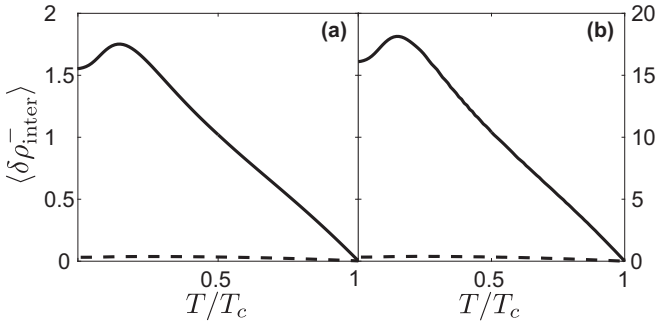

FIG. 5. Thermally averaged antisymmetrized interband **q**-integrated LDOS change $\langle\delta\rho^-_{\rm inter}\rangle(\Omega)$ for nonmagnetic scatterers with parameters $U_{\rm inter} = 0.2U_{\rm intra}$, with full t matrix. The external frequency $\Omega/T_c = 2.5$, with $|\Delta_1|/T_c$ and $|\Delta_2|/T_c$ taken as 3.0 and 2.0, respectively. (a) refers to the weak potential $U_{\rm intra} = 0.01$. Shown are antisymmetrized LDOS $\langle\delta\rho^-(\Omega)\rangle$ for s_{++} (dashed) and for $s_\pm$ state (solid). (b) shows the same for intermediate strength potential $U_{\rm intra} = 0.2$. Here we have used the standard BCS type behavior for both superconducting gaps.

D. Comparison with experiment

We have shown in the previous section that the temperature dependence of the antisymmetrized integrated LDOS is a sensitive measure of the gap sign change in a superconductor, although it does not reduce in any limit to the BCS-type temperature dependence expected from coherence factors. Here we comment on the results of Chi *et al.* [11] on LiFeAs, who neither symmetrized their integrated conductance maps, nor made use of the sign of the LDOS change, but nevertheless obtained what appeared to be a distinct qualitative result. Shown in Fig. 6 are the expected $|\langle\delta\rho_{\rm inter,intra}\rangle(\Omega)|$ for both $s_\pm$ and s_{++} states within our model, with the two gap scales indicated. While the overall behavior is somewhat complicated, one can see that it is indeed the case, as inferred by the authors of Ref. [11], that the bias dependence for an $s_\pm$ state immediately below the upper gap scale $|\Delta_h|$ is opposite for the intra- and interband contributions, while it is the same in the case of an s_{++} state. Note further that had one not known the gap scales exactly, distinguishing between the two states on the basis of this type of measurement might have been difficult: the relative magnitudes of intra-and interband contributions are probably not to be taken seriously, since it is difficult to subtract the **q** weight of the homogeneous system from the intraband. The gap scales are presumed to be known from STM experiment from direct measurements of the coherence peaks in the real space local conductance $\propto\langle\delta\rho\rangle(\mathbf{r},\Omega)$, but they will be shifted somewhat from the underlying values by thermal smearing and gap anisotropy. The former type of shift is even evident in Fig. 6. In case of more than two distinct gap values the results are even more muddled. These caveats are among the reasons why we propose that a T-dependent measurement at fixed frequency, ideally between the two gap scales, should be a more sensitive measure of the gap sign change.

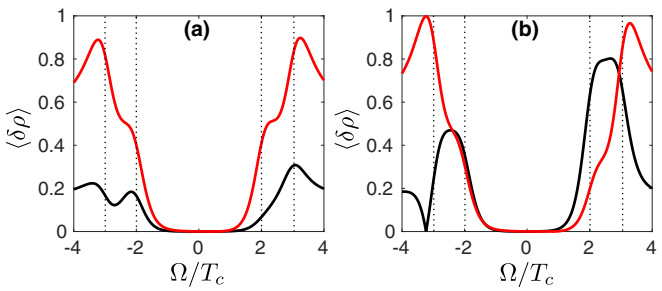

FIG. 6. (Color online) Absolute magnitude of thermally averaged *unsymmetrized* interband (black) and intraband (red) **q**-integrated LDOS changes $|\langle\delta\rho_{\rm inter,intra}\rangle(\Omega)|$ for s_{++} (a) and $s_\pm$ (b) vs Ω/T_c for nonmagnetic scatterers with parameters $T = 0.2T_c$ and $U_{\rm inter} = 0.2U_{\rm intra}$, with full t matrix, and $|\Delta_1|/T_c$ and $|\Delta_2|/T_c$ taken as 3.0 and 2.0, respectively. $\Omega = |\Delta_1|$ and $|\Delta_2|$ are indicated by dashed lines.

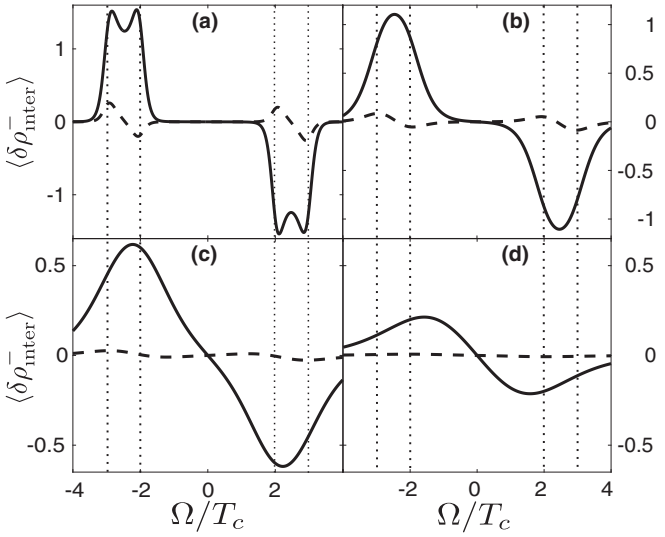

FIG. 7. Thermally averaged LDOS changes for antisymmetric, interband channel, $|\langle\delta\rho_{\rm inter,intra}\rangle(\Omega)|$ vs Ω/T_c. Curves shown are for nonmagnetic scatterers with parameters $T/T_c = 0.1$ (a), 0.3 (b), 0.6 (c), 0.9 (d) and $U_{\rm inter} = 0.2U_{\rm intra}$, with full t matrix, and $|\Delta_1|/T_c$ and $|\Delta_2|/T_c$ taken as 3.0 and 2.0, respectively. $\Omega = |\Delta_1|$ and $|\Delta_2|$ are indicated by dashed lines. Solid curve: $s_\pm$. Dashed curve: s_{++}.

To illustrate what one should expect, we now plot in Fig. 7 the antisymmetric component of the interband LDOS as a function of bias Ω, for different temperatures. This is the quantity that should show the most prominent difference between s_{++} and $s_\pm$. In particular, this component for the s_{++} case should exhibit a sign change at a frequency corresponding to the geometric mean of the two gap scales, while $s_\pm$ has a finite large value there. With further increase of the temperature, the main features decrease in amplitude but should remain detectable. We expect that this will be the typical behavior seen in experiment.

E. Effect of particle-hole asymmetry: momentum-resolved Green's functions

To complete our analysis, we also performed a calculation assuming a lattice based model with two bands, giving parabolic like electron and hole band dispersions near the Γ and the M points of the Brillouin zone. In particular, we consider the simplest band topology of the iron-based

superconductors with hole band, $\varepsilon_h(\mathbf{k}) = \mu_h - \frac{\mathbf{k}^2}{2m_h}$, centered near the Γ point of the Brillouin zone and the electron band, $\varepsilon_e(\mathbf{k}) = \frac{(\mathbf{k}+\mathbf{Q})^2}{2m_e} - \mu_e$, centered near the M point of the Brillouin zone [$\mathbf{Q}=(\pi,\pi)$]. Here, we set $\frac{1}{2m_h} = \frac{1}{2m_e} = 34$ and $\mu_e = -10.6$, $\mu_h = 9.4$ (all in the same units of energy as for the momentum independent model). The most important part introduced by the lattice based models is the electron hole asymmetry in the normal part of the Nambu Green's functions,

$$\hat{G}_\nu^0(\mathbf{k}, i\omega_n) \simeq -\frac{i\omega_n\tau_0 + \varepsilon_\nu(\mathbf{k})\tau_3 + \Delta_\nu\tau_1}{\omega_n^2 + \Delta_\nu^2 + \varepsilon_\nu^2(\mathbf{k})}. \quad (11)$$

Substituting the Green's function for the electron and hole bands, Eq. (11) into Eqs. (3), (5), and (9) we computed the interband and inraband corrections to the LDOS similar to the main text. In Figs. 8–10, we show the corresponding results for the integrated density of states components $\delta\rho^{\pm}_{\text{intra,inter}}$, thermally averaged antisymmetrized interband $\mathbf{q}$-integrated LDOS change $\langle\delta\rho^{-}_{\text{inter}}\rangle(\Omega)$, and thermally averaged LDOS changes for antisymmetric, interband channel, $|\langle\delta\rho_{\text{inter,intra}}\rangle(\Omega)|$ versus Ω/T_c, respectively. Despite some differences, the main features that allow one to distinguish s_{++} and $s_{\pm}$ superconducting gaps continue to hold also if one uses more realistic Green's functions. We believe this happens because the electron and hole Fermi surfaces and corresponding gaps are well separated in $\mathbf{q}$ space. This allows one to disentangle intra- and inter-band scattering processes in the normal and superconducting states

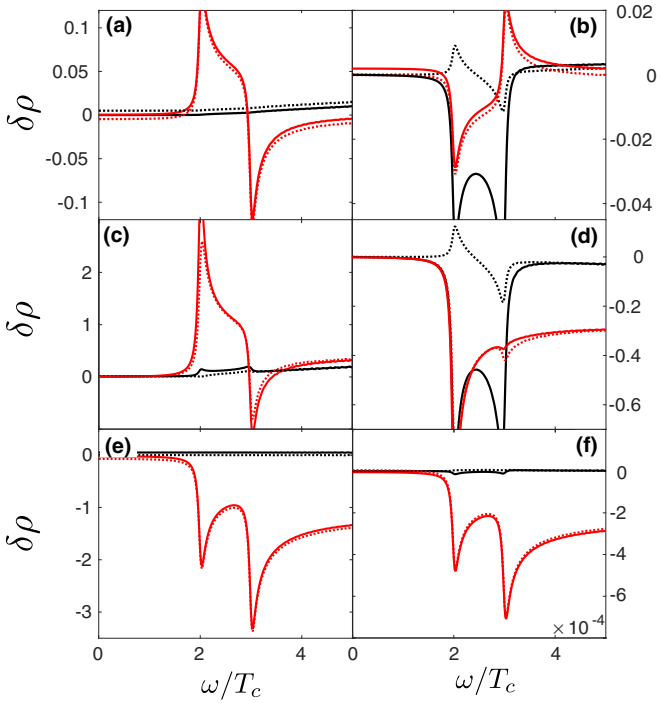

FIG. 8. (Color online) Integrated density of states components $\delta\rho^{\pm}_{\text{intra,inter}}$ for isotropic scatterers $U_{\text{inter}} = 0.2U_{\text{intra}}$ for $U_{\text{intra}} = 0.01$ [(a) and (b)], 0.2 [(c) and (d)], and 10 [(e) and (f)] (all in units of energy as in the main text), computed for momentum resolved Green's functions, Eq. (A14). As in Fig. 3, the dashed curves correspond to s_{++} state, solid curves to $s_{\pm}$. Red and black are even and odd components of the LDOS, $\delta\rho^{+}$ and $\delta\rho^{-}$, respectively. Left panels represent intraband, right panels interband scattering channels, respectively.

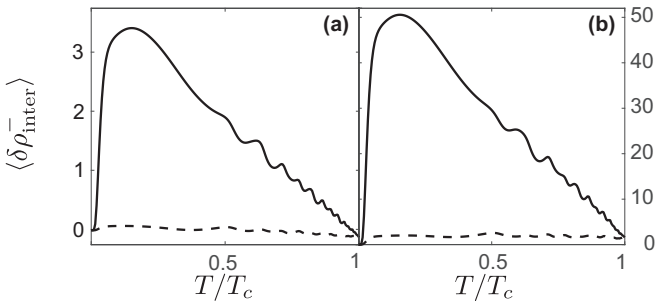

FIG. 9. Thermally averaged antisymmetrized interband $\mathbf{q}$-integrated LDOS change $\langle\delta\rho^{-}_{\text{inter}}\rangle(\Omega)$ for nonmagnetic scatterers with parameters $U_{\text{inter}} = 0.2U_{\text{intra}}$, with full t matrix and momentum resolved Green's function, Eq. (A14). The external frequency $\Omega/T_c = 2.5$, with $|\Delta_1|/T_c$ and $|\Delta_2|/T_c$ taken as 3.0 and 2.0, respectively. (a) refers to the intermediate potential $U_{\text{intra}} = 0.2$. Shown are antisymmetrized LDOS $\langle\delta\rho^{-}(\Omega)\rangle$ for s_{++} (dashed) and for $s_{\pm}$ state (solid). (b) shows the same for the larger strength potential $U_{\text{intra}} = 10$. As in Fig. 5, here we have used the standard BCS type behavior for both superconducting gaps.

clearly, as found in most of the ferropnictides. In particular, we observe that the actual T/T_c dependence for the $s_{\pm}$-wave symmetry shows a nonmonotonic dependence which is reflected in the peaklike structure at small T/T_c values and corresponding downward behavior at low T/T_c values. This is absent for the s_{++}-wave symmetry. In addition, we see from Fig. 10 that the antisymmetrized STM signal for $|\Delta_1| \lesssim \Omega \lesssim |\Delta_2|$ has one sign for $s_{\pm}$ and changes sign for s_{++}. Therefore we believe that these two key features can be observed in the experiments.

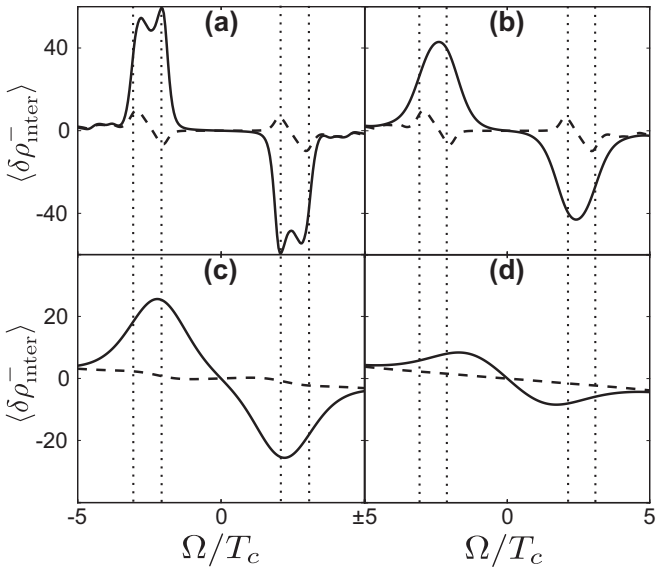

FIG. 10. Thermally averaged LDOS changes for antisymmetric, interband channel, $|\langle\delta\rho_{\text{inter,intra}}\rangle(\Omega)|$ vs Ω/T_c. Curves shown are for nonmagnetic scatterers with parameters $T/T_c = 0.1$ (a), 0.3 (b), 0.6 (c), 0.9 (d) and $U_{\text{inter}} = 0.2U_{\text{intra}}$ ($U_{\text{intra}} = 0.2$), with full t matrix, momentum-resolved Green's functions, Eq. (A14), and $|\Delta_1|/T_c$ and $|\Delta_2|/T_c$ taken as 3.0 and 2.0, respectively. $\Omega = |\Delta_1|$ and $|\Delta_2|$ are indicated by dashed lines. Solid curve: $s_{\pm}$. Dashed curve: s_{++}.

F. Remarks on magnetic and τ_1 ("vortex") scatterers

A weak "magnetic impurity" represented by an isolated classical spin that couples via exchange to conduction electron spin density may be written in Nambu space as $V_{\rm spin}\tau_0\sigma_3$, where σ_3 is the Pauli matrix in spin space. Within the Born approximation, the change to the up-spin LDOS will cancel that of the down-spin LDOS. Higher-order magnetic scatterings will produce effects, but since in general a chemical substituent with a magnetic moment will have a nonmagnetic scattering potential much larger than its magnetic one, we ignore this effect here. Including transverse spin couplings (or deep d or f levels within an Anderson model approach) will result in Kondo physics which obviously produces interesting effects on the density of states, including Kondo resonances near the Fermi level, with concomitant influence on QPI; these have been recently discussed elsewhere [27]. Similar effects on the QPI would be expected when the Yu-Shiba bound state is induced by the magnetic impurity. In order to draw qualitative conclusions regarding gap symmetry using the methods described here, samples or regions of samples displaying Kondo and/or Yu-Shiba bound state resonances should be excluded.

Scattering in the τ_1, or Andreev channel has been discussed in several contexts in the field of unconventional superconductivity. Chemical impurities suppress the order parameter in their vicinity, creating an effective off-diagonal local potential which contributes to the scattering of quasiparticles [28,29]. Normally these effects are ignored, e.g., in standard t matrix calculations, or treated as weak, but under some circumstances they can become important. If an impurity has the effect of enhancing the pairing locally, as occurs in some models [30–34], the τ_1 potential component of an impurity can be significant and even control the behavior of the conductance spectrum and map [31].

The order parameter is also suppressed near vortex cores, and Pereg-Barnea and Franz suggested that this fact could be used to provide a method of controlling disorder and distinguishing gap symmetries *in situ*, provided the vortex lattice were sufficiently disordered [6]. Here we do not discuss τ_1 chemical impurities in detail, as we are focussed primarily on qualitative aspects of QPI, but we discuss the oft-repeated statement that the effect of the disordered vortex lattice, represented by a random, tunable set of τ_1 scatterers can distinguish sign-preserving and sign-reversing QPI peaks. It is believed [7,8,11] that the peaks whose weight is enhanced in a field correspond to sign-preserving peaks, while those whose weight is suppressed by a field are sign-reversing.

In fact a clear statement to this effect is difficult to make. As we showed in Sec. III A, τ_1 impurities indeed enhance the QPI signal in the intraband channel, which represents sign-preserving scattering for both superconducting states considered. In addition, Table I also shows that the sign-preserving interband scatterings in the s_{++} case give rise to an enhancement. There is no indication of a *suppression* with field in the sign-reversing ($s_\pm$ interband) case, however. This apparent discrepancy was noted already by Pereg-Barnea and Franz [6], who suggested that the disordered vortex lattice led to a random phase potential experienced by quasiparticles, which might give rise to an overall suppression of the QPI signal. Such a "background" suppression could then be overcompensated by the singular enhancements of the sign-preserving scattering wave vectors. There is, however, no calculation to support this assertion, so statements about determining gap symmetry from QPI peaks in unconventional superconductors from their field behavior should be treated with caution (see also the discussion in Appendix).

G. Application to other states; nodeless d wave

While for pedagogical reasons we have restricted ourselves to two bands, isotropic gaps, and either s_{++} or $s_\pm$ states, the concepts we have discussed are clearly applicable to more general situations. The interband entries of Table I labeled s_{++} apply generally to gap sign preserving transitions between bands, and those labeled $s_\pm$ apply to sign-changing ones. The obvious example under discussion in the Fe-based superconductivity field is the putative d-wave state in systems with no hole pockets but four electron pockets at the $(\pm\pi,0)$ and $(0,\pm\pi)$, initially proposed for the alkali-intercalated FeSe materials [35,36]. In addition to Bragg scattering and small q intraband scattering, interband scattering should give rise to rings of scattering intensity around $\mathbf{q} = (0,\pm 2\pi)$ and $(\pm 2\pi,0)$, as well as around $(\pm 2\pi,\pm 2\pi)$. Predictions for intraband scattering weights will be identical to those listed for $s_\pm$ in Table I.

V. CONCLUSIONS

In this paper, we have argued that the task of identifying order parameter symmetries in unconventional superconductors via QPI measurements is unlikely to be successful if it relies, as in the past, on comparisons of theoretical conductance maps with experiment. This is because there are too many unknown parameters, particularly in multiband systems, to allow for a quantitative theory of QPI. It is possible that this situation can be improved to some extent by *ab initio* based calculation of the density of states away from the metal surface, including an isolated impurity. This would be however time consuming and would still not eliminate all quantitative assumptions. On the other hand, in systems like the Fe-based superconductors, where one can clearly identify QPI peaks related to intra- and interband scattering, the temperature dependence of the integrated weights of these peaks can provide a robust qualitative means of detecting order parameter sign changes that can be used to determine its structure.

We have focused our attention on a model of a two-band system with two distinct gaps Δ, and shown that the most sensitive way to distinguish scattering processes connecting gaps of same or different sign is to operate with STM bias in the energy region between the two gap scales, identification of which is a relatively simple experimental task. We have then shown that the T-dependent response of the symmetrized and anitsymmetrized combinations of the conductance for both intra- and interband scattering provide a characteristic signature of a gap sign change or lack thereof. These temperature dependencies do *not*, as suggested by previous works, correspond to thermal averages of simple BCS coherence factors, but are somewhat more complicated. In particular, we find that the effect is strongest at low temperatures, and not near T_c, in contrast to the expectation assuming coherence factors. Although we have focused on the question of distinguishing $s_\pm$ and s_{++} states in

the FeSC, it is clear that similar arguments can be made for sign-changing gaps in other contexts, for instance a putative d-wave state in FeSC materials with electron pockets only.

In the past, most QPI experiments have focused on the power spectrum of the LDOS, in other words the absolute magnitude of the density of states Fourier transform $|\delta\rho(\mathbf{q})|$ or related ratios of this quantity, so-called Z or R maps. We have shown here that measurement of the *signed* symmetrized and antisymmetrized QPI maps are crucial to extract symmetry information in the absence of detailed knowledge of the impurity potentials, which is usually the case. This effect persists up to T_c.

The existence of order parameter bound states is one aspect which must be treated with care in such a measurement, as we have shown that they tend to steal weight from the spectral region where the characteristic distinctions are most visible. Of course if one has a clear indication of a bound state induced by a nonmagnetic impurity, it is already a strong indication of a sign-changing order parameter. Nevertheless, additional complementary evidence can be obtained by performing the analysis suggested here while masking the regions containing the bound states before Fourier transforming.

Finally, we have discussed the commonly used method of distinguishing gap symmetries by observing the magnetic field dependence of QPI peaks and identifying sign-preserving scattering wave vectors as those corresponding to peaks that increase with field, and sign-changing ones with those that decrease with field. This analysis, while appealing and possibly correct in some cases, is based on a questionable analogy of vortices as pointlike Andreev scatterers that may fail for several reasons, including if the vortex lattice is too ordered or coherence lengths too large. In addition, while we can understand within the work presented here why some QPI peaks can be enhanced by the magnetic field, there is no firm theoretical ground for interpretation of those peaks that are suppressed.

ACKNOWLEDGMENTS

We thank P. Coleman, D.J. Scalapino, and I. Vekhter for useful discussions. P.J.H. was supported by NSF-DMR-1407502, and I.I.M. by the U.S. Office of Naval Research through the Naval Research Laboratory's Basic Research Program. The work of DA and IE was supported by the Focus Program 1458 Eisen-Pniktide of the DFG, and by the German Academic Exchange Service (DAAD PPP USA No. 57051534). P.J.H. and I.I.M. would like to thank for hospitality R. Valenti and the Goethe University of Frankfurt, where this project was started, as well as the Kavli Institute for Theoretical Physics, where several key discussions took place. I.E. acknowledges the support allocated to Kazan Federal University for the project part of the state assignment in the sphere of scientific activities.

APPENDIX

1. Remarks on the Bragg peaks and the 1-Fe versus 2-Fe Brillouin zone

The electronic structure of the iron-based superconductors can be described exactly in the Brillouin zone corresponding to a 2-Fe unit cell, or approximately in the twice larger one, corresponding to a 1-Fe cell [1]. In the former case, the intraband scattering create a QPI spot near the zone center ($\mathbf{q} \approx \mathbf{0}$), and an intraband one near zone corners ($\mathbf{q} \approx \pi/a,\pi/a$), where a is the lattice parameter of the 2-Fe cell, $a = d\sqrt{2}$, and d is the Fe-Fe bond length. In the experiment, the QPI signal is invariably mixed with the Bragg peaks, resulting from electrons scattering off the regular crystal lattice. It is important to understand that, just as in x-ray scattering, while the density of states $\rho(\mathbf{q})$ is peaked at each reciprocal lattice $\mathbf{G}$, the intensity of each $\mathbf{q}+\mathbf{G}$ component depends on $\mathbf{G}$, and generally decays with $|G|$, and the same is true for the QPI spectra. In other word, when we say that the intraband spot is located around $\mathbf{q} = \mathbf{0}$, it is implied that there are also spots near all $\mathbf{q} = \mathbf{G}$, albeit with a reduced intensity.

Now, let us use the 1-Fe cell, and a twice larger Brillouin zone. In this setting, there are spots near $\mathbf{q}_1 \approx 0$, near $\mathbf{q}_2 \approx \pi/d,0$, and two overlapping spots near $\mathbf{q}_{3,4} \approx \pi/d,\pi/d$. Three of them, the first one and the last two, are located at 2-Fe reciprocal lattice vectors. Of course, this means that as long as we include scattering off the pnictogen or chalcogen sublattice, each of these peaks will generate shadow peaks at all other reciprocal lattice vectors. Experimentally, however, they will be clearly distinguishable: the $\mathbf{q}_1$ peak will be most intensive at $\mathbf{G} = \mathbf{0}$, while $\mathbf{q}_{3,4}$ will actually be stronger at $\mathbf{G} = 0,\pm\pi/a$ and $\pm\pi/a,0$ (in the reduced zone). The spots near $\mathbf{q}_2$ will not be affected by the downfolding procedure, as for this particular vector the sublattice scattering will not generate any shadows.

This may seem to be of academic importance, but it may have considerable practical ramifications. Indeed, while for Fe-based superconductors, as mentioned, there is no problem separating the hole-hole and electron-electron scattering from the hole-electron one, the scattering between two inequivalent electron pockets in the 2-Fe zone is seemingly indistinguishable from the intraband scattering, and, as the latter, overlaps with the Bragg peaks. But, as discussed above, the intraband scattering will be stronger at that half of the reciprocal lattice vectors that coincide with those reciprocal lattice vectors of the 1-Fe cell, while the interband electron-electron scattering will be stronger at the other half of the $\mathbf{G}$ vectors. This, of course, makes the signatures of the order parameter signs discussed in the main text weaker, but does not destroy them. Moreover, several papers recently suggested a possibility of the order parameter sign change between different hole bands [37,38] in particular, between the two bands formed by the xz and yz orbitals and the one with predominantly xy character. In the 2-Fe zone, they both occur at the zone center and thus seem indistinguishable. However, a closer look reveals that the first two bands generate a spot that is located at the zone center in both 1-Fe and 2-Fe zones, while the scattering between xz/yz and xy pockets, in the 1-Fe zone occurs near the zone corner. While both processes will create "shadows" at all 2-Fe reciprocal lattice vectors, the former will be stronger at one half of the vectors, and the other at the other half, again allowing to use QPI to assess the above hypothesis.

Finally, the very fact that some of the nontrivial QPI spots are overlapping with Bragg peaks is not a disadvantage, but

just the opposite. As pointed out by Hanaguri *et al.* [8], the Bragg peaks are much sharper then the QPI maxima, and have distinctly different profiles, which allows them to be separated. Note that the mechanism that is supposed to generate a QPI dependence on the external magnetic field should not operate on the Bragg peaks, whether in the normal or superconducting state. Thus, if not only the QPI, but also the Bragg peaks demonstrate a strong field dependence (as was in fact the case in Ref. [8]), this strongly suggests that the field dependence of the QPI spectra is also not directly related to scattering off Abrikosov vortices. Given the caveats described in the main text, this capability appears rather useful.

2. Coherence factors

We remarked in the introduction that there is an expectation shared by many in the STM community that the temperature and bias dependence of QPI signals will follow simple BCS coherence factors. This is based in part on Refs. [7] and [23], which expressed the change in the Fourier transform density of states as an integral over such factors, written explicitly, for instance, for the antisymmetrized response and Born scattering, as $(u_{\mathbf{k}}u_{\mathbf{k}'} - v_{\mathbf{k}}v_{\mathbf{k}'})^2$, and similar expressions for other types of scattering. However, this assertion is not correct and the prefactors in the expressions for the QPI intensity cannot be cast into such form. Let us illustrate that now for the Born scattering. In this case,

$$\delta\rho(\mathbf{q},\omega) = \frac{1}{2}Tr\,\mathrm{Im}\int_{\mathbf{k}} \tau_3 G_{\mathbf{k}}(\omega)\tau_3 G_{\mathbf{k}'}(\omega)\delta(\mathbf{k}-\mathbf{k}'-\mathbf{q}) \tag{A1}$$

$$= \mathrm{Im}\int_{\mathbf{k}} \frac{\omega^2 + \xi_{\mathbf{k}}\xi_{\mathbf{k}+\mathbf{q}} - \Delta_{\mathbf{k}}\Delta_{\mathbf{k}'}}{\left(\omega^2 - E_{\mathbf{k}}^2\right)\left(\omega^2 - E_{\mathbf{k}'}^2\right)}\delta(\mathbf{k}-\mathbf{k}'-\mathbf{q}), \tag{A2}$$

where ξ are the one-electron energies. Concentrating on the fraction under the integral, we see that it is

$$\begin{aligned}
\mathrm{Im}\,\frac{\omega^2 + \xi_{\mathbf{k}}\xi_{\mathbf{k}} - \Delta_{\mathbf{k}}\Delta_{\mathbf{k}}}{\left(\omega^2 - E_{\mathbf{k}}^2\right)\left(\omega^2 - E_{\mathbf{k}'}^2\right)} &= \mathrm{Im}(\omega^2 + \xi_{\mathbf{k}}\xi_{\mathbf{k}'} - \Delta_{\mathbf{k}}\Delta_{\mathbf{k}'})\Bigg[\mathrm{Im}\,\frac{1}{4E_{\mathbf{k}}}\left(\frac{1}{\omega - E_{\mathbf{k}}} - \frac{1}{\omega + E_{\mathbf{k}'}}\right)\mathrm{Re}\,\frac{1}{\left(\omega^2 - E_{\mathbf{k}'}^2\right)} \\
&\quad + \mathrm{Im}\,\frac{1}{4E_{\mathbf{k}'}}\left(\frac{1}{\omega - E_{\mathbf{k}'}} - \frac{1}{\omega + E_{\mathbf{k}'}}\right)\mathrm{Re}\,\frac{1}{\left(\omega^2 - E_{\mathbf{k}}^2\right)}\Bigg] \\
&= \left[\frac{\delta(\omega - E_{\mathbf{k}})\left(E_{\mathbf{k}}^2 + \xi_{\mathbf{k}}\xi_{\mathbf{k}'} - \Delta_{\mathbf{k}}\Delta_{\mathbf{k}'}\right)}{4E_{\mathbf{k}}\left(E_{\mathbf{k}}^2 - E_{\mathbf{k}'}^2\right)} + \frac{\delta(\omega - E_{\mathbf{k}'})\left(E_{\mathbf{k}'}^2 + \xi_{\mathbf{k}}\xi_{\mathbf{k}'} - \Delta_{\mathbf{k}}\Delta_{\mathbf{k}'}\right)}{4E_{\mathbf{k}'}\left(E_{\mathbf{k}'}^2 - E_{\mathbf{k}}^2\right)}\right] \\
&= \frac{1}{\left(E_{\mathbf{k}}^2 - E_{\mathbf{k}'}^2\right)}\left[\frac{\delta(\omega - E_{\mathbf{k}})\left(E_{\mathbf{k}}^2 + \xi_{\mathbf{k}}\xi_{\mathbf{k}'} - \Delta_{\mathbf{k}}\Delta_{\mathbf{k}'}\right)}{4E_{\mathbf{k}}} - \frac{\delta(\omega - E_{\mathbf{k}'})\left(E_{\mathbf{k}'}^2 + \xi_{\mathbf{k}}\xi_{\mathbf{k}'} - \Delta_{\mathbf{k}}\Delta_{\mathbf{k}'}\right)}{4E_{\mathbf{k}'}}\right].
\end{aligned} \tag{A3}$$

Note that arguments of the δ functions are different, therefore in order to combine the two terms we need to rename the $\mathbf{k}$ variables in the second term, after which, assuming inversion symmetry in Δ and ξ, we get

$$\begin{aligned}
\delta\rho(\mathbf{q},\omega) &= \int_{\mathbf{k}}\left[\frac{\delta(\omega - E_{\mathbf{k}})\left(E_{\mathbf{k}}^2 + \xi_{\mathbf{k}}\xi_{\mathbf{k}'} - \Delta_{\mathbf{k}}\Delta_{\mathbf{k}'}\right)}{8E_{\mathbf{k}}\left(E_{\mathbf{k}}{}^2 - E_{\mathbf{k}'}^2\right)} + \frac{\delta(\omega - E_{\mathbf{k}'})\left(E_{\mathbf{k}'}^2 + \xi_{\mathbf{k}}\xi_{\mathbf{k}'} - \Delta_{\mathbf{k}}\Delta_{\mathbf{k}'}\right)}{4E_{\mathbf{k}'}\left(E_{\mathbf{k}'}^2 - E_{\mathbf{k}}^2\right)}\right]\delta(\mathbf{k}-\mathbf{k}'-\mathbf{q}) \\
&= \int_{\mathbf{k}}\frac{\left(E_{\mathbf{k}}^2 + \xi_{\mathbf{k}}\xi_{\mathbf{k}'} - \Delta_{\mathbf{k}}\Delta_{\mathbf{k}'}\right)\delta(\omega - E_{\mathbf{k}})}{\left(E_{\mathbf{k}}^2 - E_{\mathbf{k}'}^2\right)\omega}\frac{\delta(\mathbf{k}-\mathbf{k}'-\mathbf{q})}{2}.
\end{aligned} \tag{A4}$$

The first factor is what was taken to be a coherence factor in Refs. [7] and [23]. However, the true coherence factor in question is different, namely, $(E_{\mathbf{k}}^2 + \xi_{\mathbf{k}}\xi_{\mathbf{k}'} - \Delta_{\mathbf{k}}\Delta_{\mathbf{k}'})/(E_{\mathbf{k}}E_{\mathbf{k}'})$, that instead of the expression above one would have a very different formula, namely

$$\int_{\mathbf{k}}\frac{(\omega^2 + \xi_{\mathbf{k}}\xi_{\mathbf{k}'} - \Delta_{\mathbf{k}}\Delta_{\mathbf{k}'})\delta(\omega - E_{\mathbf{k}})\delta(\omega - E_{\mathbf{k}'})}{\omega^2}\frac{\delta(\mathbf{k}-\mathbf{k}'-\mathbf{q})}{2} \neq \int_{\mathbf{k}}\frac{(\omega^2 + \xi_{\mathbf{k}}\xi_{\mathbf{k}'} - \Delta_{\mathbf{k}}\Delta_{\mathbf{k}'})\delta(\omega - E_{\mathbf{k}})}{\omega\left(\omega^2 - E_{\mathbf{k}'}^2\right)}\frac{\delta(\mathbf{k}-\mathbf{k}'-\mathbf{q})}{2}. \tag{A5}$$

One may think that this difference will disappear after an integration over **q,** and the integrated expression will be similar to classic BCS predictions of thermally averaged transition probabilities, e.g., in NMR spin relaxation and/or ultrasonic attenuation [39]. For example, consider the spin-lattice relaxation rate

$$\frac{1}{T_1T} \propto \lim_{\omega_0\to 0}\sum_{\mathbf{q},\mu,\nu}\frac{\mathrm{Im}\chi^{\mu\nu}(\mathbf{q},\omega_0)}{\omega_0} \simeq \lim_{\omega_0\to 0}\frac{1}{\omega_0}\mathrm{Im}\sum_{\mathbf{k},\mathbf{k}',\mu,\nu}\mathrm{Tr}(\hat{\alpha}\hat{G}^0(\mathbf{k},\omega_n)\hat{\alpha}\hat{G}^0(\mathbf{k}',\omega_n+\omega_0))_{i\omega_0\to\omega_0+i0^+}, \tag{A6}$$

where χ is the spin susceptibility matrix in band space, $\hat{\alpha}$ is the electronic spin operator in Nambu space, ω_0 is the Larmor frequency, and we have neglected any momentum dependence of hyperfine matrix elements in order to arrive at a simple expression. In fact, Eq. (A6) bears a certain resemblance to the structure of Eq. (1), in particular because each Green's function is local and therefore integrated over momentum independently. Performing these sums and the analytical continuation, one obtains

the usual result, with slight generalization to multiband systems:

$$\begin{aligned}\frac{1}{T_1T} &\propto \sum_{\mu,\nu}\int_0^\infty d\omega\left(-\frac{\partial f}{\partial\omega}\right)\left[\mathrm{Im}\left(\frac{\omega}{\sqrt{\Delta_\mu^2-\omega^2}}\right)\mathrm{Im}\left(\frac{\omega}{\sqrt{\Delta_\nu^2-\omega^2}}\right)+\mathrm{Im}\left(\frac{\Delta_\mu}{\sqrt{\Delta_\mu^2-\omega^2}}\right)\mathrm{Im}\left(\frac{\Delta_\nu}{\sqrt{\Delta_\nu^2-\omega^2}}\right)\right]\\ &= \text{intrabandterms}+2\int_0^\infty d\omega\left(-\frac{\partial f}{\partial\omega}\right)\left[\mathrm{Im}\left(\frac{\omega}{\sqrt{\Delta_h^2-\omega^2}}\right)\mathrm{Im}\left(\frac{\omega}{\sqrt{\Delta_e^2-\omega^2}}\right)+\mathrm{Im}\left(\frac{\Delta_h}{\sqrt{\Delta_h^2-\omega^2}}\right)\mathrm{Im}\left(\frac{\Delta_e}{\sqrt{\Delta_e^2-\omega^2}}\right)\right]\\ &= \text{intrabandterms}+2\int_{\max(\Delta_h,\Delta_e)}^\infty d\omega\left(-\frac{\partial f}{\partial\omega}\right)\frac{\omega^2+\Delta_h\Delta_e}{\sqrt{\omega^2-\Delta_h^2}\sqrt{\omega^2-\Delta_e^2}}.\end{aligned}\tag{A7}$$

Now one can see that an s_{++} superconductor will have an interband contribution to NMR relaxation that obeys exactly a BCS type II coherence factor T dependence (in the limit $\Delta_h\to\Delta_e$), while for $s_\pm$, the corresponding result is type I.

Compare now to our expression for the interband contribution to the Fourier transform density of states in the case of a weak potential scatterer, Eq. (7), together with the thermal average,

$$\begin{aligned}\langle\delta\rho_{\text{inter}}(\omega)\rangle &\propto \int d\omega\left(-\frac{\partial f}{\partial\omega}\right)\mathrm{Im}\frac{\omega^2-\Delta_h\Delta_e}{\sqrt{\omega^2-\Delta_h^2}\sqrt{\omega^2-\Delta_e^2}}\\ &= \int_{\Delta_e}^{\Delta_h} d\omega\left(-\frac{\partial f}{\partial\omega}\right)\frac{\omega^2-\Delta_h\Delta_e}{\sqrt{\Delta_h^2-\omega^2}\sqrt{\omega^2-\Delta_e^2}}.\end{aligned}\tag{A8}$$

We see that while the functional form of the fraction under the integral is indeed the same, the cost of the **q** integration is that the frequency integral is now taken over a totally different, in fact not overlapping, limits, which results in a completely different T dependence, as shown above.

3. Single impurity t matrix for two-band system

The t matrix for a single impurity is given by

$$\underline{t}=\left[1-\underline{U}\tau_3\sum_{\mathbf{k}}\underline{G}(\mathbf{k},\omega)\right]^{-1}\tau_3\underline{U},\tag{A9}$$

where the integrated matrix Green's function given in Eq. (4) can be further rewritten as $(\sum_{\mathbf{k}}\underline{G}(\mathbf{k},\omega))_\nu=g_{\omega,\nu}\tau_0+g_{\Delta,\nu}\tau_1$ for each of the band. The scattering matrix $\underline{U}$ can be then separated into intraband $(\underline{U})_{\nu\nu}=U_{\text{intra}}$ and interband $(\underline{U})_{\mu\nu}=U_{\text{inter}}$ term.

Inverting the t matrix, one finds the common denominator for both intra- and interband terms of the t matrix

$$D=-\left(g_{\omega,h}^2-g_{\Delta,h}^2\right)U_{\text{intra}}^2-\left(g_{\omega,e}^2-g_{\Delta,e}^2\right)U_{\text{intra}}^2-2(g_{\omega,h}g_{\omega,e}-g_{\Delta,h}g_{\Delta,e})U_{\text{inter}}^2+\left(g_{\omega,h}^2-g_{\Delta,h}^2\right)\left(g_{\omega,2}^2-g_{\Delta,2}^2\right)\left(U_{\text{inter}}^2-U_{\text{intra}}^2\right)^2+1.\tag{A10}$$

Now for the intraband scattering within the band 1 one obtains in Nambu components

$$\hat{t}_h=t_h^0\tau_0+t_h^1\tau_1+t_h^3\tau_3\tag{A11}$$

with

$$\begin{aligned}t_h^0&=\left[g_{\omega,h}U_{\text{intra}}^2+g_{\omega,e}U_{\text{inter}}^2-g_{\omega,h}\left(g_{\omega,e}^2-g_{\Delta,e}^2\right)\left(U_{\text{inter}}^2-U_{\text{intra}}^2\right)^2\right]/D,\\ t_h^1&=\left[-g_{\Delta,h}U_{\text{intra}}^2-g_{\Delta,e}U_{\text{inter}}^2+g_{\Delta,h}\left(g_{\omega,e}^2-g_{\Delta,e}^2\right)\left(U_{\text{inter}}^2-U_{\text{intra}}^2\right)^2\right]/D,\\ t_h^3&=\left[U_{\text{intra}}\left(1-\left(g_{\omega,e}^2-g_{\Delta,e}^2\right)\left(U_{\text{intra}}^2-U_{\text{inter}}^2\right)\right)\right]/D.\end{aligned}\tag{A12}$$

The expressions for $\hat{t}_e$ are obtained by exchanging the band indices h and e. Similarly, the interband t matrix can be written as

$$\hat{t}_{eh}=t_{eh}^0\tau_0+t_{eh}^1\tau_1+t_{eh}^2\tau_2+t_{eh}^3\tau_3\tag{A13}$$

with

$$\begin{aligned}t_{eh}^0&=[(g_{\omega,e}+g_{\omega,h})U_{\text{intra}}U_{\text{inter}}]/D\\ t_{eh}^1&=[-(g_{\Delta,e}+g_{\Delta,h})U_{\text{intra}}U_{\text{inter}}]/D\\ t_{eh}^2&=\left[-i(g_{\Delta,e}g_{\omega,h}-g_{\omega,e}g_{\Delta,h})U_{\text{inter}}\left(U_{\text{inter}}^2-U_{\text{intra}}^2\right)\right]/D\\ t_{eh}^3&=\left[U_{\text{inter}}(g_{\omega,e}g_{\omega,h}-g_{\Delta,e}g_{\Delta,h})\left(U_{\text{intra}}^2-U_{\text{inter}}^2\right)+1\right]/D,\end{aligned}\tag{A14}$$

and the corresponding expression for t_{he}. Note that the interband scattering terms generate a τ_2 contribution for the interband t matrix.

[1] P. J. Hirschfeld, M. M. Korshunov, and I. I. Mazin, Rep. Prog. Phys. **74**, 124508 (2011).
[2] I. I. Mazin, D. J. Singh, M. D. Johannes, and M. H. Du, Phys. Rev. Lett. **101**, 057003 (2008).
[3] H. Kontani and S. Onari, Phys. Rev. Lett. **104**, 157001 (2010).
[4] S. Maiti, M. M. Korshunov, T. A. Maier, P. J. Hirschfeld, and A. V. Chubukov, Phys. Rev. Lett. **107**, 147002 (2011).
[5] T. S. Nunner, W. Chen, B. M. Andersen, A. Melikyan, and P. J. Hirschfeld, Phys. Rev. B **73**, 104511 (2006).
[6] T. Pereg-Barnea and M. Franz, Phys. Rev. B **78**, 020509 (2008).
[7] T. Hanaguri, Y. Kohsaka, M. Ono, M. Maltseva, P. Coleman, I. Yamada, M. Azuma, M. Takano, K. Ohishi, and H. Takagi, Science **323**, 923 (2009).
[8] T. Hanaguri, S. Niitaka, K. Kuroki, and H. Takagi, Science **328**, 474 (2010).
[9] F. Wang, H. Zhai, and D.-H. Lee, Phys. Rev. B **81**, 184512 (2010).
[10] A. Akbari, J. Knolle, I. Eremin, and R. Moessner, Phys. Rev. B **82**, 224506 (2010).
[11] S. Chi, S. Johnston, G. Levy, S. Grothe, R. Szedlak, B. Ludbrook, R. Liang, P. Dosanjh, S. A. Burke, A. Damascelli, D. A. Bonn, W. N. Hardy, and Y. Pennec, Phys. Rev. B **89**, 104522 (2014).
[12] A. Kreisel, P. Choubey, T. Berlijn, W. Ku, B. M. Andersen, and P. J. Hirschfeld, Phys. Rev. Lett. **114**, 217002 (2015).
[13] L. Capriotti, D. J. Scalapino, and R. D. Sedgewick, Phys. Rev. B **68**, 014508 (2003).
[14] L. Zhu, W. A. Atkinson, and P. J. Hirschfeld, Phys. Rev. B **69**, 060503 (2004).
[15] P. T. Sprunger, L. Petersen, E. W. Plummer, E. Lægsgaard, and F. Besenbacher, Science **275**, 1764 (1997).
[16] J. E. Hoffman, K. McElroy, D. H. Lee, K. M. Lang, H. Eisaki, S. Uchida, and J. C. Davis, Science **297**, 1148 (2002).
[17] S. Sykora and P. Coleman, Phys. Rev. B **84**, 054501 (2011).
[18] T. Hänke, S. Sykora, R. Schlegel, D. Baumann, L. Harnagea, S. Wurmehl, M. Daghofer, B. Büchner, J. van den Brink, and C. Hess, Phys. Rev. Lett. **108**, 127001 (2012).
[19] F. Wang, H. Zhai, and D. H. Lee, Europhys. Lett. **85**, 37005 (2009).
[20] E. Plamadeala, T. Pereg-Barnea, and G. Refael, Phys. Rev. B **81**, 134513 (2010).
[21] Y. Y. Zhang, C. Fang, X. Zhou, K. Seo, W. F. Tsai, B. A. Bernevig, and J. Hu, Phys. Rev. B **80**, 094528 (2009).
[22] Q.-H. Wang and D.-H. Lee, Phys. Rev. B **67**, 020511 (2003).
[23] M. Maltseva and P. Coleman, Phys. Rev. B **80**, 144514 (2009).
[24] D. V. Efremov, M. M. Korshunov, O. V. Dolgov, A. A. Golubov, and P. J. Hirschfeld, Phys. Rev. B **84**, 180512 (2011).
[25] J. E. Hoffman, Rep. Prog. Phys. **74**, 124513 (2011).
[26] R. Beaird, I. Vekhter, and J.-X. Zhu, Phys. Rev. B **86**, 140507 (2012).
[27] M. A. Derry, A. K. Mitchell, and D. Logan, Phys. Rev. B **92**, 035126 (2015).
[28] M. H. Hettler and P. J. Hirschfeld, Phys. Rev. B **59**, 9606 (1999).
[29] A. Shnirman, I. Adagideli, P. M. Goldbart, and A. Yazdani, Phys. Rev. B **60**, 7517 (1999).
[30] I. N. Khlyustikov and A. I. Buzdin, Adv. Phys. **36**, 271 (1987).
[31] T. S. Nunner, B. M. Andersen, A. Melikyan, and P. J. Hirschfeld, Phys. Rev. Lett. **95**, 177003 (2005).
[32] M. M. Maśka, Z. Śledź, K. Czajka, and M. Mierzejewski, Phys. Rev. Lett. **99**, 147006 (2007).
[33] K. Foyevtsova, R. Valentí, and P. J. Hirschfeld, Phys. Rev. B **79**, 144424 (2009).
[34] K. Foyevtsova, H. C. Kandpal, H. O. Jeschke, S. Graser, H.-P. Cheng, R. Valentí, and P. J. Hirschfeld, Phys. Rev. B **82**, 054514 (2010).
[35] F. Wang, F. Yang, M. Gao, Z.-Y. Lu, T. Xiang, and D.-H. Lee, Europhys. Lett. **93**, 57003 (2011).
[36] T. A. Maier, S. Graser, P. J. Hirschfeld, and D. J. Scalapino, Phys. Rev. B **83**, 100515 (2011).
[37] Z. P. Yin, K. Haule, and G. Kotliar, Nat. Phys. **10**, 845 (2014).
[38] F. Ahn, I. Eremin, J. Knolle, V. B. Zabolotnyy, S. V. Borisenko, B. Büchner, and A. V. Chubukov, Phys. Rev. B **89**, 144513 (2014).
[39] M. Tinkham, *Introduction to Superconductivity*, 2nd ed. Dover Books in Physics, (Dover Publications, Mineola, NY, 2004).